

## **Contents of this file**

### **S1. Supplementary text**

- S1.1 Model configuration and simulation setup
- S1.2 Model equations for detrital tracers
- S1.3 Estimation of POC concentration from bio-optical data
- S1.4 Evaluation of vertical POC fluxes against sediment trap data

### **S2. Supplementary tables**

- S2.1 PISCES parameters for detrital tracers.
- S2.2 Processes contributing to detrital POC budgets in PISCES.
- S2.3 Evaluation metrics for monthly mean data in each region

### **S3. Supplementary figures**

- S3.1 Evaluation of the mean seasonal cycle of the mixed layer depth (MLD)
- S3.2 Seasonal maps of modelled MLD compared to the Ifremer reanalysis
- S3.3 Seasonal maps of modelled NPP compared to a satellite product
- S3.4 Latitudinal profile of the POC/bbp700 ratio used to estimate POC from gridded bpp700
- S3.5 Seasonal cycles of *sdetoc* budgets in the mesopelagic layer
- S3.6 Seasonal cycles of *ldetoc* budgets in the mesopelagic layer

### **S4. Additional Supporting Information (Files uploaded separately) (spreadsheets)**

- S4.1 Annual mean vertical flux profiles and additional modelled variables quoted in the text.
- S4.2 Monthly and annual mesopelagic detritus budgets by region.

### **S1. Supplementary text**

#### **S1.1 Model configuration and simulation setup**

We use the dynamical ocean model NEMO 4.0.4 (Nucleus for European Modelling of the Ocean; Madec, 2008), coupled with the sea-ice model SI3 (Vancoppenolle et al., 2009) and the biogeochemical model PISCESv2\_RC (Pelagic-Interactions Scheme for Carbon and Ecosystem Studies; Aumont et al., 2015, 2017). NEMO and PISCES are coupled through the Tracers in Ocean Paradigm (TOP) tracer manager (NEMO TOP Working Group, 2018), which performs advective and diffusive transports of both physical and biogeochemical tracers. The same advection scheme, named second-order Flux Corrected Transport (FCT) (Lévy et al., 2001), is used for all tracers for consistency. Lateral diffusion is performed with a forward Laplacian operator. Vertical diffusion (mixing) is parameterised using the turbulent kinetic energy (TKE) closure scheme; convection triggered by unstable stratification is represented with an enhanced vertical diffusion scheme, and re-stratification by mixed-layer eddies is represented with the Fox-Kemper parameterisation (NEMO System Team, 2019).

Global simulations were run on the ORCA1L75 grid, with ca. one-degree horizontal resolution and 75 non-linear vertical levels (of which 24 were in the top 100 m and 22 were between 100-1000 m depth), and with a 45-minute time step for both ocean dynamics and biogeochemistry. The NEMO-PISCES simulation followed the Ocean Model Intercomparison Project protocol (OMIP-2; Tsujino et al., 2018) using JRA-55 reanalysis (Kobayashi et al., 2015) as atmospheric forcing. The simulation repeated six cycles of the 62-year (1958–2019) JRA55 forcing dataset. The first two cycles consisted of NEMO-only simulations, and PISCES was coupled at the beginning of the third cycle. A biogeochemical spin-up was performed by cycling 21 times through the same ocean circulation, corresponding to the third cycle (21-cycle x 62-year = 1302 years) while letting the biogeochemical tracers equilibrate. The atmospheric CO<sub>2</sub> concentration was fixed at a preindustrial level corresponding to 1850. At the end of the biogeochemical spin-up, global net primary production (PP) and gravitational export at 100 m stabilised respectively at 50.8 PgC yr<sup>-1</sup> and 6.86 PgC yr<sup>-1</sup> and changed by less than 0.01% over successive cycles. After the spin-up, the simulation proceeded with the remaining three cycles, with a prescribed rise in atmospheric CO<sub>2</sub> concentrations during the last 170 years of the simulation matching the one observed over the 1850-2019 period. Only results from the last cycle (1958–2019) are analysed here, focusing on the North Atlantic.

## S1.2 Model equations for detrital tracers

Below we reproduce the prognostic equations for the *sdetoc* and *ldetoc* tracers, which in the model are internally named *POC* and *GOC*, respectively. Corresponding parameter values are listed in Table S1. These equations include gravitational sinking, which is computed by PISCES, but not the advective and diffusive transport terms, which are computed by TOP.

The equations shown in Aumont et al. (2015) do not fully reflect the model equations in NEMO version 4.0.4. Here we provide updated equations for the budget terms corresponding to mesozooplankton flux feeding (which removes both POC and GOC) and fragmentation (which transfers GOC to POC). The mesozooplankton flux feeding and fragmentation terms are expanded below the main budget equations. We also corrected the quadratic mortality terms of small phytoplankton and diatoms, which in eq. 37 and 40 of Aumont et al. (2015) were not multiplied by the shear rate (*sh*). In the case of diatoms, the aggregation term was not included in eq. 40. These terms are described in greater detail below.

At each PISCES time step, the *POC* tracer (E. 37 in Aumont et al., 2015) is updated as:

$$\begin{aligned}
\frac{\partial POC}{\partial t} = & \sigma^Z \Sigma g^Z(X)Z + 0.5m^D \frac{D}{D + K_m} D + r^Z f_Z \frac{Z}{Z + K_m} Z + m^Z f_Z(T)Z^2 \\
& + (1 - 0.5R_{CaCO_3}) \left( m^P \frac{P}{P + K_m} P + sh\omega^P P^2 \right) + s_{GOC} GOC + F_{FF}^M \\
& + \phi_1^{DOC} + \phi_3^{DOC} - (g^M(POC) - g_{FF}^M(POC))M - g^Z(POC)Z \\
& - k_{POC} POC - \phi - \omega_{POC} \frac{\partial POC}{\partial Z}
\end{aligned}$$

(Eq. S1)

Likewise, the *GOC* tracer (Eq. 40 in Aumont et al., 2015) is updated as:

$$\begin{aligned}
\frac{\partial GOC}{\partial t} = & \sigma^M \left( \sum_l g^M(l) + g_{FF}^M(POC) + g_{FF}^M(GOC) \right) M + r^M f_M(T) \frac{M}{M + K_m} M + P_{up}^M \\
& + 0.5R_{CaCO_3} \left( m^P \frac{P}{P + K_m} P + sh\omega^P P^2 \right) + 0.5m^D \frac{D}{D + K_m} D \\
& + sh(\omega^D + \omega_{max}^D \lim_D) D^2 + \phi + \phi_2^{DOC} - g_{FF}^M(GOC)M - F_{FF}^M \\
& - s_{GOC} GOC - k_{GOC} GOC - \omega_{GOC} \frac{\partial GOC}{\partial Z}
\end{aligned}$$

(Eq. S2)

Where:

- $Z, M, P$  and  $D$  is, respectively, the concentration (biomass) of the microzooplankton, mesozooplankton, small phytoplankton and diatom tracer.
- $\sigma$  is the unassimilated fraction of microzooplankton or mesozooplankton ingestion, as indicated by the superscript.
- $\Sigma g^Z(X)$  and  $\Sigma g^M(X)$  are, respectively, microzooplankton and mesozooplankton total ingestion. Microzooplankton ingestion occurs only in “standard” phagotrophic predation mode, with  $X$  corresponding to  $P, D$  and  $POC$ . Mesozooplankton ingestion is the sum of “standard” ingestion of  $P, D, M$  and  $POC$ , plus flux feeding ingestion of  $POC$  and  $GOC$  (represented by the  $g_{FF}^M$  coefficient, expanded below)
- $r^Z$  and  $r^M$  are, respectively, the linear mortality parameters of micro- and mesozooplankton
- $m^Z$  and  $m^M$  are, respectively, the quadratic mortality parameters of micro- and mesozooplankton
- $P_{up}^M$  is the fraction of mesozooplankton quadratic mortality that results in faecal pellet production (the remainder is respired).  $P_{up}^M$  is proportional to  $\sigma^M m^M M^2$  and is further modulated by the maximum mesozooplankton gross growth efficiency under the assumption of an infinite chain of carnivores

(Anderson et al., 2013). The full formulation of this term is in Eq. 30 and 31 of Aumont et al. (2015).

- $K_m$  is the half-saturation constant for mortality, which acts to avoid extinction of  $Z$  or  $M$  when their biomass is very low
- $m^P$  and  $m^D$  are, respectively, the linear mortality parameters of small phytoplankton and diatoms
- $\omega^P$  and  $\omega^D$  are, respectively, the quadratic mortality parameters of small phytoplankton and diatoms. These parameters must be multiplied by the shear rate  $sh$ , which is  $1 \text{ s}^{-1}$  in the mixed layer and  $0.01 \text{ s}^{-1}$  below it, resulting in much faster aggregation within the mixed layer.
- $\omega_{max}^D$  is the maximum quadratic mortality of diatoms, representing coagulation into large aggregates upon nutrient exhaustion. This term additionally multiplies the function  $lim_D = 0.25(1 - L_D^2)/(0.25 + L_D^2)$ , where  $L_D$  is diatom nutrient limitation ( $L_D = 1$  means no limitation and sets  $lim_D$  to 0).
- $R_{CaCO_3}$  is the fraction of small phytoplankton calcifiers, also called rain ratio, which in PISCES is an empirical function of temperature, light (PAR), mixed layer depth, and the  $r_{CaCO_3}$  parameter (Eq. 77 in Aumont et al., 2015).
- $sgoc$  represents microbially-induced GOC disaggregation, also referred to as solubilization, which accounts for the bacterial enzymatic activity that breaks down the exopolymers that bind aggregates together. The value of this coefficient is fixed at  $sgoc = (0.04/2.56) * 1/(1 - 50^{-0.04}) = 0.108$ . According to the PISCESv2\_RC code, the value of  $solgoc$  “is based on a fractal dimension of 2.56 and a spectral slope of -3.6 (identical to what is used in p4zsink [routine] to compute aggregation)”. This term was not described by Aumont et al. (2015) but appears in the PISCESv2\_RC code released with NEMO4.0.4. Conversely, the  $\lambda^*_{POC GOC}$  in Eq. 37 and 40 (Aumont et al., 2015) is not found in the PISCES version we used.
- $\phi_1^{DOC}$  and  $\phi_2^{DOC}$  are the rates of turbulence (shear) induced aggregation of DOC into POC and GOC, respectively;  $\phi_3^{DOC}$  is the rate of Brownian aggregation of DOC into POC;  $\phi$  represents aggregation of POC to GOC due to turbulence and differential settling. These terms are controlled by parameters  $a_1$  to  $a_9$ , as described in Eq. 36 and 39 in Aumont et al. (2015). For simplicity and owing to the comparatively low rate of these processes,  $a_1$ – $a_9$  parameters are not listed in Table S1.
- $g^M$  is the rate of microzooplankton phagotrophic (“standard”) feeding on POC.

Its formulation is analogous to all other zooplankton “standard” feeding terms, described in eq. in Aumont et al. (2015).

- $g_{FF}^M(POC)$  and  $g_{FF}^M(GOC)$  are the rates of mesozooplankton flux feeding on POC and GOC, respectively, and are expanded in the equations below.
- $F_{FF}^M$  is the rate of GOC fragmentation to POC due to mesozooplankton flux feeding (expanded below)
- $k_{POC}$  and  $k_{GOC}$  are, respectively, the mass-specific POC and GOC decay rates, which are not model parameters, but the result of the variable reactivity parameterisation as described by Aumont et al. (2017). Their maximal value is set through the namelist parameter *xremip*, which by default is  $0.035 \text{ d}^{-1}$ .
- $\omega_{POC}$  and  $\omega_{GOC}$  are, respectively, the sinking velocities of POC and GOC.

The rates of mesozooplankton flux feeding on POC and GOC are formulated as:

$$g_{FF}^M(POC) = \text{grazflux} \omega_{POC} POC (1 - \Delta O_2) p_{FF}^M \quad (\text{Eq. S3a})$$

$$g_{FF}^M(GOC) = \text{grazflux} \omega_{GOC} GOC (1 - \Delta O_2) p_{FF}^M \quad (\text{Eq. S3b})$$

where is the mesozooplankton flux feeding parameter, formally representing a *grazflux* biomass-normalized cross section. It has dimensions of area per unit mesozooplankton biomass. The value of this parameter is set to  $3 \text{ m}^2 (\text{mol C})^{-1}$ . However, since PISCES code internally uses units of  $\text{mol L}^{-1}$ , this parameter takes an equivalent value of  $3000 \text{ L m}^{-1} (\text{mol C})^{-1}$  in the PISCES namelist. The decrease in these rates caused by oxygen deficiency is represented by, which varies between 0 (fully oxic conditions) and 1  $\Delta O_2$  (anoxia), as described in Eq. 57 of Aumont et al. (2015).

The proportion of mesozooplankton flux feeders,  $p_{FF}^M$ , depends on the flux feeding rates themselves. Thus, it must be iteratively diagnosed at each model time step:  $g_{FF}^M$  is first calculated assuming  $p_{FF}^M = 1$ ; then  $p_{FF}^M$  is estimated as the ratio between flux feeding and total mesozooplankton ingestion rates, including flux feeding,

$$p_{FF}^M = \frac{g_{FF}^M(POC) + g_{FF}^M(GOC)}{\Sigma g^M(X)} \quad (\text{Eq. S4})$$

and the final rates are computed by multiplying the initial ones by the updated value of  $p_{FF}^M$ .

Fragmentation of large detritus by mesozooplankton is expressed as a function of flux feeding rates and the ratio between biogenic silica (BSi) and GOC tracers. Modulation of fragmentation by biogenic silica implicitly accounts for the increased porosity and

fragility of large detritus when they are composed of diatom aggregates.

$$F_{FF}^M = \text{grazflux} \omega_{GOC} GOC p_{FF}^M \frac{0.2+3.8(BSi/GOC)^2}{1^2+(BSi/GOC)^2} \quad (\text{Eq. S5})$$

### S1.3 Estimation of POC concentration from bio-optical data

We compared our model's POC outputs to observational estimates based on the MULTIOBS\_GLO\_BIO\_BGC\_3D\_REP\_015\_010 product from Copernicus Marine Environmental Monitoring Service - CMEMS (Sauzède et al., 2016)(last accessed on August 2023). This product is based on a neural network algorithm that generates monthly gridded 3D fields of particulate backscattering at 700 nm wavelength ( $b_{bp,700}$ ) as a function of remotely sensed ocean colour (reflectance) and hydrological properties. Particulate backscattering profiles were converted into POC using two different methods: Galí et al. (2022) and Koestner et al. (2024), hereafter G22 and K24.

The G22 method prescribes a variable  $POC/b_{bp,700}$  ratio in the upper mixed layer as a function of geographic location and mixed layer depth (MLD). This ratio then decreases asymptotically between the base of the mixed layer and 1000 m, where it reaches a constant  $POC/b_{bp,700}$  of 1000 mmol C m<sup>-2</sup>. Here, we modified G22 such that the sea-surface  $POC/b_{bp,700}$  ratio was estimated as a continuous, smooth function of latitude, instead of being assigned a regional value (Fig. S4). To calculate the smooth  $POC/b_{bp,700}$  latitudinal profile, we built on the processing described by Galí et al. (2022) with some extra-steps. Briefly, we

- 1) binned the BGC-Argo  $b_{bp,700}$  dataset (all profiles until January 2020) into a monthly climatology on the ORCA2\_L31 horizontal-vertical grid, computing the median, mean and maximum value in each bin,
- 2) screened out grid cells where the maximum  $b_{bp,700}$ , averaged over the top 50 m, exceeded 0.008 m<sup>-1</sup> or the 98% percentile of the entire dataset,
- 3) masked out grid cells outside the “mean biomes” as per Fay & McKinley, (2014), and also the Mediterranean Sea
- 4) used this cleaned global dataset to compute, for each grid cell, the annual monthly maximum of the bin medians, means and maxima (2-degrees resolution),
- 5) computed a mean latitudinal profile of the monthly maxima “ $bbp700\_max\_LatProf$ ” (based on bin medians) and smoothed it with a 10-degrees-window rolling median
- 6) using the linear relationship between  $bbp700\_max$  and the POC vs.  $b_{bp,700}$  slope across regions (as per figure A1 of Galí et al., 2022), we recast the  $bbp700\_max\_LatProf$  into POC units to obtain a latitudinal profile of the  $POC/b_{bp,700}$  ratio. We assumed 0-intercept in the POC vs.  $b_{bp,700}$  regression.
- 7) fitted the latitudinal profiles of the  $POC/b_{bp,700}$  ratio using, consecutively, a piecewise linear regression with 4 breakpoints (at latitudes -60, -28, 38 and 50), and a smoothing spline function (10-degrees window)
- 8) Finally, used this idealised spline function of latitude to obtain the sea-surface  $POC/b_{bp,700}$  ratio, corresponding to a+c in Eq. 1 of Galí et al. (2022).

The K24 method (Koestner et al., 2024) estimates POC as a multivariate function of  $b_{bp,700}$  and chlorophyll concentration, such that the  $POC/b_{bp,700}$  ratio increases with increasing chlorophyll/ $b_{bp,700}$  ratio. The latter parameter is thought to account for particle freshness or lability, implying higher  $bbp$ -specific POC content. Here we used K24 equations between the

surface and the bottom of the euphotic layer (Morel et al., 2007). Below the euphotic layer, where chlorophyll concentration is not available, we prescribed the same asymptotic decrease in  $\text{POC}/b_{\text{bp},700}$  ratios towards 1000 m as in G22. However, given that K24 was developed using data from the epipelagic layer, mesopelagic K24 data suffer from greater uncertainty (see also figure 13 in Koestner et al., 2024).

As a final note, the POC estimate included in the CMEMS dataset was based on the equation  $\text{POC} = 38687.27 \text{ } b_{\text{bp}}^{0.95}$ . In mesopelagic waters,  $b_{\text{bp},700}$  typically ranges between  $10^{-4}$  and  $10^{-3} \text{ m}^{-1}$ . Using that equation, POC concentration would range between 6.1 and  $54.6 \text{ mg m}^{-3}$ , corresponding to  $\text{POC}/b_{\text{bp},700}$  ratios of 61000 to 54000. These ratios are comparable to the highest ones found in oligotrophic high-latitude surface waters (Galí et al., 2022; Figure A1), but by no means representative of the mesopelagic layer —where  $\text{POC}/b_{\text{bp},700}$  ratios decrease sharply with depth (Bol et al., 2018).

#### **S1.4 Evaluation of vertical POC fluxes against sediment trap data**

We compared PISCES output to a compilation of in situ POC vertical fluxes measured with sediment traps (Mouw et al., 2016a). To this end, we selected trap deployments whose duration was between 1 and 33 days. These measurements were matched to model output from the corresponding location (horizontal grid cell), depth (model vertical level), year, and month. The merged dataset was bin-averaged by region and layer, as shown in the legend of Fig. 6. Although the layers used for binning are somewhat arbitrary, they approximately correspond to the epipelagic (0–150), upper mesopelagic (100–500), lower mesopelagic (500–1200), and bathypelagic layers (1200–4000). Instead of the usual definition of 1000 m as the base of the mesopelagic layer, we set the boundary at 1200 m to be able to include in the lower mesopelagic layer a large number of data from sediment traps deployed at around 1100 m at the BATS/OFP site. BATS/OFP is the best-documented study site in the dataset, and excluding it would significantly reduce the amount of evaluation data.

#### **Supplementary references**

Anderson, T. R., Hessen, D. O., Mitra, A., Mayor, D. J., & Yool, A. (2013). Sensitivity of

secondary production and export flux to choice of trophic transfer formulation in marine ecosystem models. *Journal of Marine Systems*, 125, 41–53.

<https://doi.org/10.1016/j.jmarsys.2012.09.008>

Aumont, O., Ethé, C., Tagliabue, A., Bopp, L., & Gehlen, M. (2015). PISCES-v2: An ocean

biogeochemical model for carbon and ecosystem studies. *Geoscientific Model Development*, 8(8), 2465–2513. <https://doi.org/10.5194/gmd-8-2465-2015>

- Aumont, O., Van Hulten, M., Roy-Barman, M., Dutay, J.-C., Éthé, C., & Gehlen, M. (2017). Variable reactivity of particulate organic matter in a global ocean biogeochemical model. *Biogeosciences*, 14(9), 2321–2341. <https://doi.org/10.5194/bg-14-2321-2017>
- Bol, R., Henson, S. A., Rumyantseva, A., & Briggs, N. (2018). High-Frequency Variability of Small-Particle Carbon Export Flux in the Northeast Atlantic. *Global Biogeochemical Cycles*, 32(12), 1803–1814. <https://doi.org/10.1029/2018GB005963>
- Fay, A. R., & McKinley, G. A. (2014). Global open-ocean biomes: Mean and temporal variability. *Earth System Science Data*, 6(2), 273–284. <https://doi.org/10.5194/essd-6-273-2014>
- Galí, M., Falls, M., Claustre, H., Aumont, O., & Bernardello, R. (2022). Bridging the gaps between particulate backscattering measurements and modeled particulate organic carbon in the ocean. *Biogeosciences*, 19(4), 1245–1275. <https://doi.org/10.5194/bg-19-1245-2022>
- Koestner, D., Stramski, D., & Reynolds, R. A. (2024). Improved multivariable algorithms for estimating oceanic particulate organic carbon concentration from optical backscattering and chlorophyll-a measurements. *Frontiers in Marine Science*, 10, 1197953. <https://doi.org/10.3389/fmars.2023.1197953>
- Lévy, M., Estublier, A., & Madec, G. (2001). Choice of an advection scheme for biogeochemical models. *Geophysical Research Letters*, 28(19), 3725–3728. <https://doi.org/10.1029/2001GL012947>
- Morel, A., Huot, Y., Gentili, B., Werdell, P. J., Hooker, S. B., & Franz, B. A. (2007). Examining the consistency of products derived from various ocean color sensors in open ocean (Case 1) waters in the perspective of a multi-sensor approach. *Remote Sensing of Environment*, 111(1), 69–88. <https://doi.org/10.1016/j.rse.2007.03.012>



Mouw, C. B., Barnett, A., McKinley, G. A., Gloege, L., & Pilcher, D. (2016). *Global Ocean Particulate Organic Carbon flux merged with satellite parameters* (p. 6 datasets)

[Application/zip]. PANGAEA. <https://doi.org/10.1594/PANGAEA.855600>

Sauzède, R., Claustre, H., Uitz, J., Jamet, C., Dall’Olmo, G., D’Ortenzio, F., Gentili, B., Poteau, A., & Schmechtig, C. (2016). A neural network-based method for merging ocean color and Argo data to extend surface bio-optical properties to depth: Retrieval of the particulate backscattering coefficient. *Journal of Geophysical Research: Oceans*, 121(4), 2552–2571. <https://doi.org/10.1002/2015JC011408>

## S2. Supplementary tables

**Table S2.1.** Model parameters for the *sdetoc* (=POC) and *ldetoc* (=GOC) tracers.

Parameter	Units	Value	Description
$\sigma^I$	-	0.30	Zooplankton unassimilated fraction (Z, M)
$r^Z, r^M$	$d^{-1}$	0.03; 0.005	Zooplankton linear mortality (Z, M)
$m^Z, m^M$	$(\mu\text{mol C L}^{-1})^{-1} d^{-1}$	0.004; 0.03	Zooplankton quadratic mortality (Z, M)
$m^P, m^D$	$d^{-1}$	0.01	Phytoplankton linear mortality (P, D)
$\omega^P, \omega^D$	$(\text{mol C})^{-1} d^{-1}$	0.01	Phytoplankton quadratic mortality (P, D)
$\omega_{\text{max}}^D$	$(\text{mol C})^{-1} d^{-1}$	0.03	Maximum quadratic mortality of diatoms
$K_m$	$\mu\text{mol C L}^{-1}$	0.2	Half-saturation constant for mortality
$r_{\text{CaCO}_3}$	-	0.3	Rain ratio parameter
$\text{sol}_{\text{goc}}$	$d^{-1}$	0.108	GOC solubilization
$\text{graz}_{\text{flux}}$	$\text{L m}^{-1} (\text{mol C})^{-1}$	3000	Biomass-normalized flux feeding cross section of mesozooplankton <sup>a</sup>
$\text{xremip}$	$d^{-1}$	0.035	Maximal specific decay rate of detritus
$\omega_{\text{POC}}$	$\text{m d}^{-1}$	2	POC sinking velocity
$\omega_{\text{GOC}}$	$\text{m d}^{-1}$	50	GOC sinking velocity

<sup>a</sup>See text for an equivalent parameter value in simpler units.

**Table S2.2** Biogeochemical and physical processes in PISCES contributing to the detrital POC budgets. The three columns correspond to the names in the budget equations, the nomenclature inside the model code and a brief description of the process, respectively. The terms in *italics* correspond to the terms that interconvert *sdetoc* and *ldetoc* and are repeated in both budgets. The colour of the budget terms in the right column indicates whether they are sources (red), sinks (blue) or related to transport (purple), matching the colour code of Figure 1.

SMALL DETRITUS ( <i>sdetoc</i> ) BUDGET		
schema nomenclature	variable name in PISCES	variable description
<b>mortalities<sup>1</sup></b>	mort2sdetoc	Mortalities of non-calcifying small phytoplankton, linear diatom mortality (50%), linear and quadratic microzooplankton mortalities
<b>zmicro non-assimilation<sup>2</sup></b>	zmicronoassim	Unassimilated fraction (30%) of total microzooplankton ingestion
<b>bacterial breakdown of <i>ldetoc</i><sup>3</sup></b>	ldetoc2sdetoc	Large detritus breakdown, representing bacterial solubilization of aggregate-binding polymers
<b>DOC aggregation<sup>4</sup></b>	doc2sdetoc	DOC aggregation by Brownian motion, shear and differential settling
<b>zmeso fragmentation of <i>ldetoc</i><sup>5</sup></b>	zmesofragmldetoc	Fragmentation of large detritus by mesozooplankton flux feeding
<b>zmicro ingestion<sup>6</sup></b>	zmicroingestsdetoc	Microzooplankton “standard” ingestion
<b>zmeso ingestion &amp; flux feeding<sup>7</sup></b>	zmesoingestffsdetoc	Mesozooplankton “standard” ingestion and flux feeding
<b>remineralization<sup>8</sup></b>	remsdetoc	Microbial degradation (to DOC)
<b><i>sdetoc</i> aggregation<sup>9</sup></b>	sdetoc2ldetocagg	Aggregation by turbulent coagulation and differential settling
<b>ADV<sub>L</sub><sup>10</sup></b>	xadsdetoc and yadsdetoc	Divergence of the lateral advection flux
<b>ADV<sub>Z</sub><sup>11</sup></b>	zadsdetoc	Divergence of the vertical advection fluxes
<b>DIFF<sub>L</sub><sup>12</sup></b>	ldfsdetoc	Divergence of the lateral diffusion flux
<b>DIFF<sub>Z</sub><sup>13</sup></b>	zdfsdetoc	Divergence of the vertical diffusion fluxes
<b>GS<sup>14</sup></b>	trdexpsdetoc	Divergence of the gravitational sinking flux

### LARGE DETRITUS (*ldetoc*) BUDGET

schema nomenclature	variable in the model	variable description
<b>mortalities<sup>15</sup></b>	mort2ldetoc	Mortalities of calcifying small phytoplankton, linear diatom mortality (50%), quadratic diatom mortality (enhanced aggregation upon bloom demise), linear and quadratic <sup>(a)</sup> mesozooplankton mortalities
<b>zmeso non-assimilation<sup>16</sup></b>	zmesonoassim	Unassimilated fraction (30%) of total mesozooplankton ingestion
<b><i>sdetoc aggregation<sup>9</sup></i></b>	sdetoc2ldetocagg	Small detritus aggregation into large detritus by turbulence, coagulation and settling
<b>DOC aggregation<sup>17</sup></b>	doc2ldetoc	DOC aggregation into large detritus by shear and differential settling
<b>zmeso flux feeding<sup>18</sup></b>	zmesoffldetoc	Mesozooplankton flux feeding
<b><i>zmeso fragmentation of ldetoc<sup>5</sup></i></b>	zmesofragmldetoc	Fragmentation of large detritus by mesozooplankton flux feeding
<b>remineralization<sup>19</sup></b>	remldetoc	Microbial degradation (to DOC)
<b><i>bacterial breakdown of ldetoc<sup>3</sup></i></b>	ldetoc2sdetoc	Large detritus breakdown, representing bacterial solubilization of aggregate-binding polymers
<b>ADV<sub>L</sub><sup>20</sup></b>	xadldetoc and yadldetoc	Divergence of the lateral advection fluxes
<b>ADV<sub>Z</sub><sup>21</sup></b>	zadldetoc	Divergence of the vertical advection flux
<b>DIFF<sub>L</sub><sup>22</sup></b>	ldfldetoc	Divergence of the lateral diffusion fluxes
<b>DIFF<sub>Z</sub><sup>23</sup></b>	zdfldetoc	Divergence of the vertical diffusion flux
<b>GS<sup>24</sup></b>	trdexpldetoc	Divergence of the gravitational sinking flux

<sup>a</sup>The quadratic mortality of mesozooplankton is a closure term that represents respiration and defecation of an infinite chain of carnivores. Only the fraction representing defecation (fecal pellets) enters the *ldetoc* budget (Aumont et al., 2015).

**Table S2.3.** Evaluation metrics for the monthly mean data in each region: observation mean  $\pm$  standard deviation (Obs Mean  $\pm$  std), mean relative bias (MRB), relative unbiased root mean squared error (rURMSE) and Pearson correlation coefficient (R). Units of NPP and sPOC stocks metrics are  $\text{mmol m}^{-2} \text{d}^{-1}$ , and units of MLD are m.

	SPNA				Trans_Area				STNA			
	Obs Mean $\pm$ std	MRB %	rURMSE %	R	Obs Mean $\pm$ std	MRB %	rURMSE %	R	Obs Mean $\pm$ std	MRB %	rURMSE %	R
NPP Model vs ESA	28.8 $\pm$ 18.6	-24.2	40	1	37.8 $\pm$ 8.5	-7.1	80	0.95	34.6 $\pm$ 4.4	-52.6	120	0.11
sPOC epi Model vs G22	325.1 $\pm$ 160.2	-18.2	30	0.94	270.3 $\pm$ 42.3	6.1	50	0.97	228.8 $\pm$ 6.6	-38.0	350	0.003
sPOC epi Model vs K24	532.4 $\pm$ 108.2	-50.0	40	0.97	434.8 $\pm$ 38.6	-34.0	120	0.63	356.6 $\pm$ 4.3	-60.2	540	-0.19
sPOC upper meso Model vs G22	237.8 $\pm$ 21.2	-11.4	170	0.92	251.8 $\pm$ 31.4	-35.8	30	0.94	219.1 $\pm$ 7.3	-18.5	90	0.64
sPOC upper meso Model vs K24	353.3 $\pm$ 34.0	-40.3	240	-0.65	378.1 $\pm$ 31.9	-57.2	70	0.76	378.0 $\pm$ 22.3	-52.8	70	0.81
MLD Model vs Ifremer	94.1 $\pm$ 83.8	-2.1	20	0.97	54.8 $\pm$ 38.0	-5.6	20	0.98	39.6 $\pm$ 15.3	2.5	30	0.96

### S3. Supplementary Figures

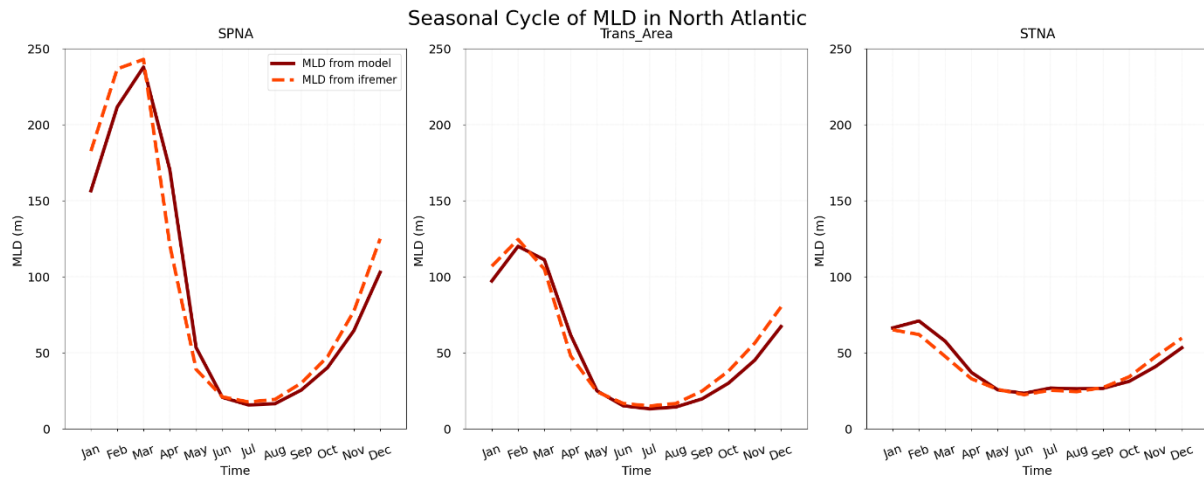


**Figure S3.1:** Seasonal cycle of the mixed layer depth (MLD) across North Atlantic regions, comparing the model to the Ifremer reanalysis.

# MLD MODEL & Difference Model-ifremer Seasonal Climatology 1998-2019 (m)

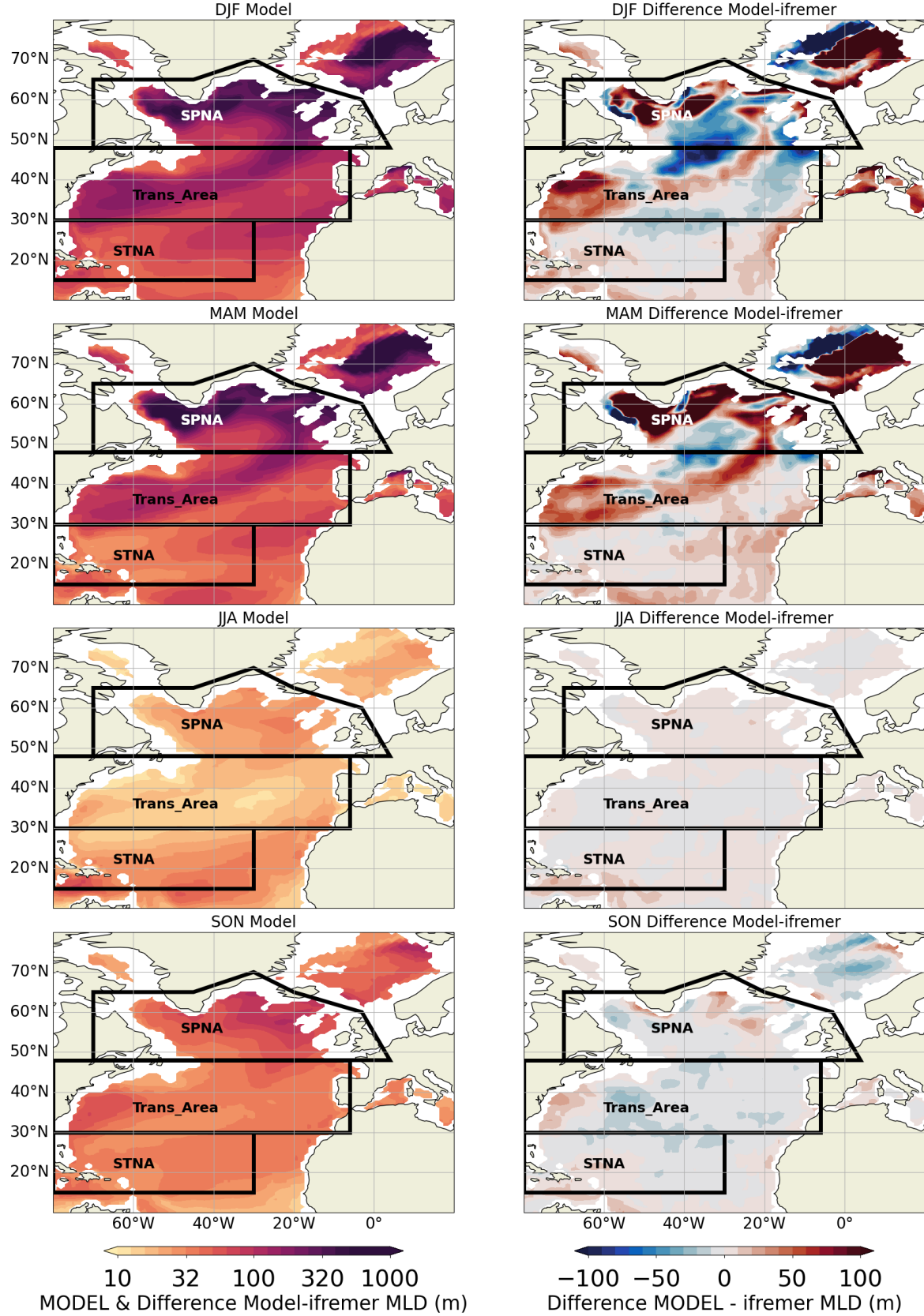


**Figure S3.2.** Seasonal maps of the mixed layer depth (MLD) simulated by the model (left) and difference between the model and the Ifremer reanalysis (right). See the text for details.



# NPP MODEL & ESA Seasonal Climatology 1998-2019 ( $\text{mmol m}^{-2} \text{d}^{-1}$ )

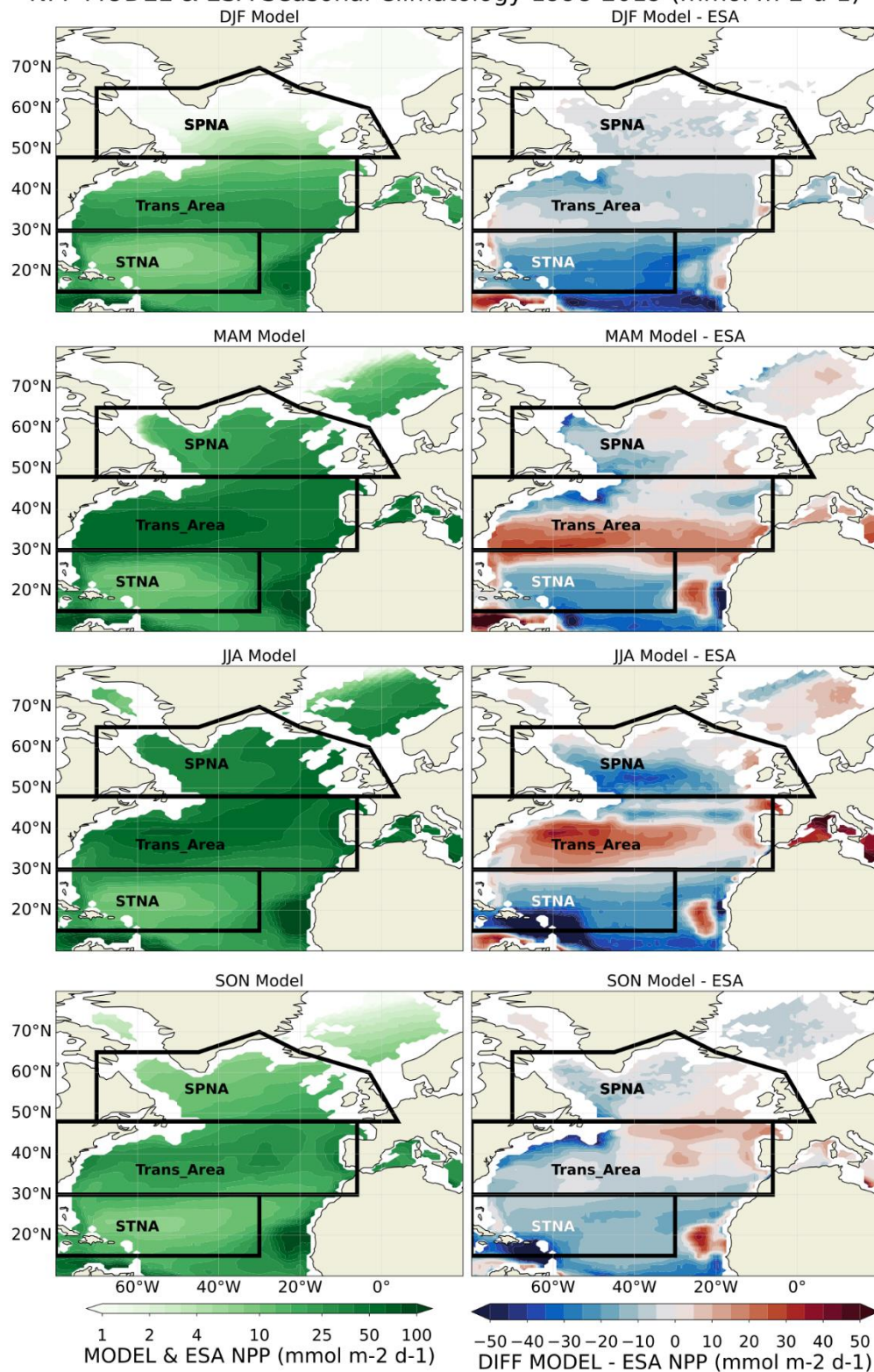


**Figure S3.3.** Seasonal maps of the vertically integrated net primary production (NPP) from the model simulation (left) and the difference between the model and a satellite estimate (right). The satellite product is the Ocean Colour Climate Change Initiative v4.2 from ESA.



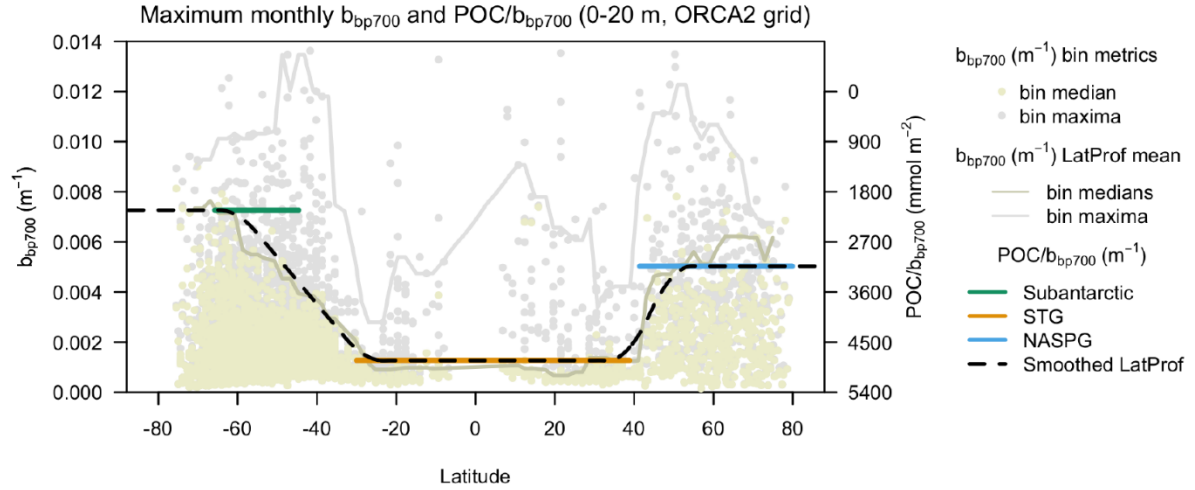


**Figure S3.4.** Smoothed latitudinal profile of the  $POC/bbp700$  ratio, used to estimate  $POC$  from gridded  $bbp700$  data. Dots show the median (beige) and maximum (grey)  $bbp700$  in  $2^\circ \times 2^\circ$  longitude-latitude bins, with lines of the same colour showing the corresponding latitudinal profiles smoothed with a  $10^\circ$  running median. Horizontal coloured lines show the regionally-fixed  $POC/bbp700$  ratios used by Galí et al. (2022), and the dashed black line is the continuous function of latitude used here to obtain  $POC/bbp700$  (right axis).

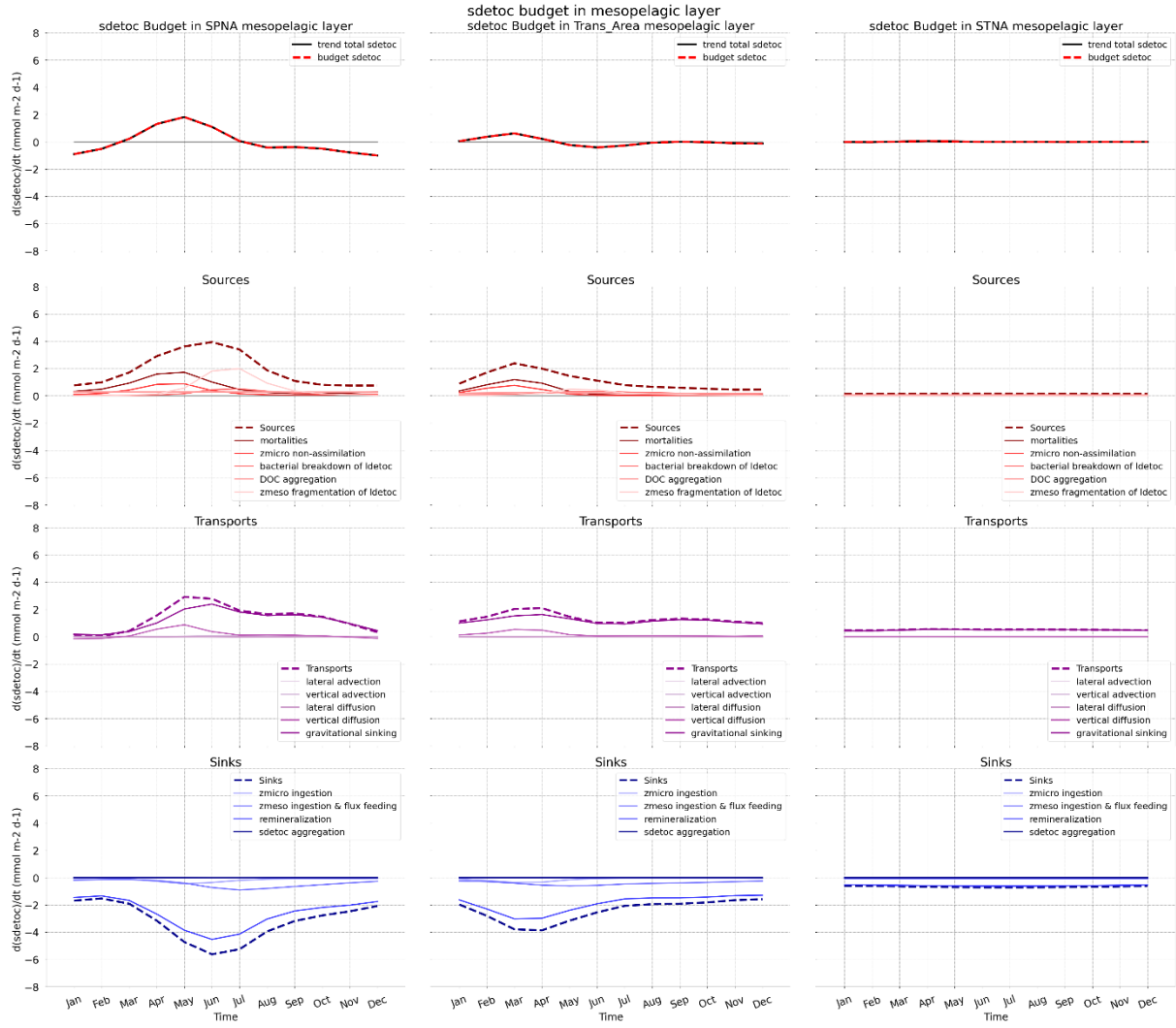


**Figure S3.5.** Seasonal cycles of *sdetoc* budgets in the mesopelagic layer (from *Zprod* to 1000m of each region): SPNA (left), *Trans\_Area* (center) and STNA (right). Rows correspond to total tracer trend (first), sources (second), transports (third) and sinks (fourth).

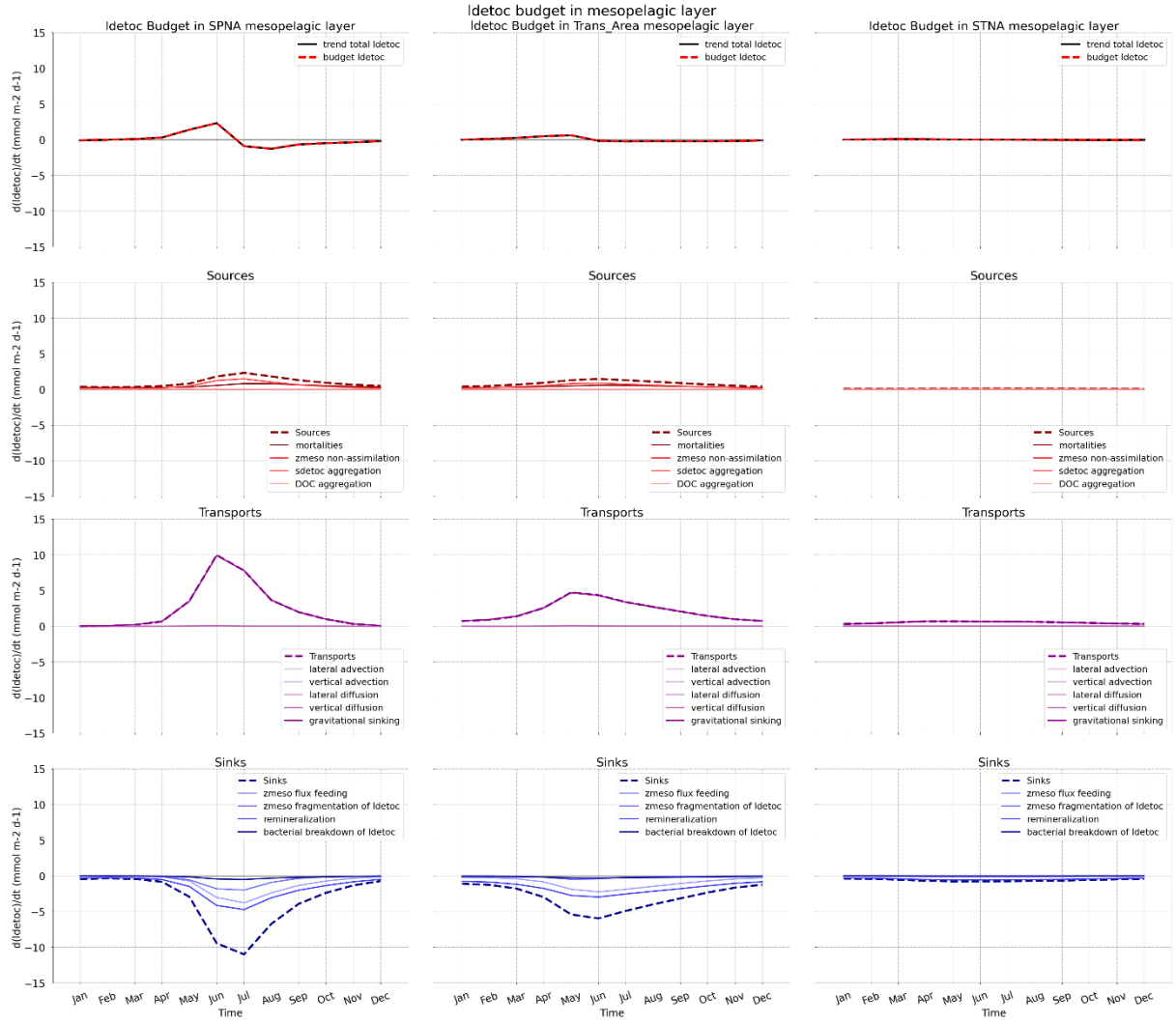


**Figure S3.6.** Seasonal cycles of Idetoc budgets in the mesopelagic layer (from Zprod to 1000m of each region): SPNA (left), Trans\_Area (center) and STNA (right). Rows correspond to total tracer trend (first), sources (second), transports (third) and sinks (fourth).